

# Diversity Analysis for Indoor Terahertz Communication Systems under Small-Scale Fading

Almutasem Bellah Enad<sup>†</sup>, Jihad Fahs<sup>†</sup>, Hakim Jemaa<sup>\*</sup>, Hadi Sarieddeen<sup>†</sup>, Tareq Y. Al-Naffouri<sup>\*</sup>

<sup>†</sup>Department of Electrical and Computer Engineering, American University of Beirut, Beirut, Lebanon,

Email: {aae118@mail.aub.edu, jihad.fahs@aub.edu.lb, hadi.sarieddeen@aub.edu.lb}

<sup>\*</sup>Department of Computer, Electrical and Mathematical Sciences and Engineering, KAUST, Kingdom of Saudi

Email: {hakim.jemaa@kaust.edu.sa, tareq.alnaffouri@kaust.edu.sa}

**Abstract**—Harnessing diversity is fundamental to wireless communication systems, particularly in the terahertz (THz) band, where severe path loss and small-scale fading pose significant challenges to system reliability and performance. In this paper, we present a comprehensive diversity analysis for indoor THz communication systems, accounting for the combined effects of path loss and small-scale fading, with the latter modeled as an  $\alpha - \mu$  distribution to reflect THz indoor channel conditions. We derive closed-form expressions for the bit error rate (BER) as a function of the reciprocal of the signal-to-noise ratio (SNR) and propose an asymptotic expression. Furthermore, we validate these expressions through extensive simulations, which show strong agreement with the theoretical analysis, confirming the accuracy and robustness of the proposed methods. Our results show that the diversity order in THz systems is primarily determined by the combined effects of the number of independent paths, the severity of fading, and the degree of channel frequency selectivity, providing clear insights into how diversity gains can be optimized in high-frequency wireless networks.

**Index Terms**—THz communications, bit-error probability, diversity,  $\alpha - \mu$  distribution.

## I. INTRODUCTION

The terahertz (THz) spectrum, spanning from 100 gigahertz (GHz) to 10 terahertz (THz), is set to revolutionize future wireless communications by supporting ultra-high data rates in the terabits-per-second range and achieving exceptionally low latency [1], [2]. THz signal propagation exhibits significant temporal and spatial sparsity [3], [4], while still enabling effective communication in non-line-of-sight (non-LoS) conditions, as evidenced by recent experiments [3]. However, even in indoor settings, non-LoS paths are generally limited, and their availability further decreases under high-gain antenna directivity [4]. Measurement-based studies have shown that the  $\alpha - \mu$  distribution provides a robust model for the magnitude of small-scale fading in indoor THz environments [5]. Unlike classical fading models such as the Nakagami-m and Rician distributions, which often fail to capture the intricate characteristics of correlated THz channels, the  $\alpha - \mu$  model offers a flexible parameterization that has demonstrated promising fitting performance [5]. This model has been instrumental in constructing an analytical framework for indoor THz propagation, as presented in [6], accounting for the additional effect of misalignment fading using the zero-boresight approach. Diversity techniques play a crucial role in

enhancing the reliability and performance of wireless systems [7]. In particular, leveraging diversity in THz communications is important to mitigate the challenges posed by severe path loss, molecular absorption, and small-scale fading [1]. Spatial, frequency, and polarization diversity methods [7], [8] can thus mitigate multipath sparsity and improve link robustness in the THz band. However, existing studies on diversity in THz channels often rely on oversimplified models that overlook realistic propagation characteristics [9], [10], leaving a gap in analyses based on accurate THz channel assumptions. In this paper, we analyze diversity assuming a maximum ratio combiner (MRC) receiver and under an  $\alpha - \mu$  distributed THz small-scale fading magnitude. We analyze how the probability of error,  $\text{Pr}_e$ , for a maximum likelihood (ML) receiver varies with the signal-to-noise ratio (SNR) over  $L \geq 1$  channel uses. We provide a complete characterization of  $\text{Pr}_e$  as a function of SNR, and show that, to first order approximation,  $\text{Pr}_e(\text{SNR}) = \kappa_1 \text{SNR}^{-\kappa_2}$ , where  $\kappa_2 = \frac{\alpha\mu}{2}L$  and  $\kappa_1$  is a method-dependent constant. Throughout the paper, the  $|\cdot|$  operator represents the absolute value,  $\mathbb{E}[\cdot]$  is the expectation operator, and  $\text{Pr}(\cdot)$  is the probability operator.  $\Gamma(\cdot)$  is the gamma function and  $\gamma(\cdot, \cdot)$  is the lower incomplete gamma function defined as:  $\gamma(\zeta, u) = \int_0^u t^{\zeta-1} e^{-t} dt$ .  $Q(x) = \frac{1}{\sqrt{2\pi}} \int_x^\infty e^{-\frac{u^2}{2}} du$  is the  $Q$ -function and  $\text{erf}(x) = \frac{2}{\sqrt{\pi}} \int_0^x e^{-u^2} du$  is the error function [11].  $G_{p,q}^{m,n} \left[ z \left| \begin{smallmatrix} a_1, \dots, a_p \\ b_1, \dots, b_q \end{smallmatrix} \right. \right]$  represents the Meijer G-function [11, eq. (9.301)] while  $H_{p,q}^{m,n} \left[ z \left| \begin{smallmatrix} (a_1, b_1), \dots, (a_p, b_p) \\ (c_1, d_1), \dots, (c_p, d_p) \end{smallmatrix} \right. \right]$  represents the Fox H-function [12, eq. (1.1.1)].

## II. SYSTEM AND CHANNEL MODELS

We consider a single-input, single-output (SISO) single-carrier THz link of complex baseband equivalent received signal [13],

$$r = h x + n, \quad (1)$$

where  $r$  is the received symbol,  $x$  is the modulated transmitted symbol,  $n$  is the additive white gaussian noise of power  $N_0/2$  ( $N_0$  is the one-sided noise power spectral density). Let  $\nu = \sqrt{P_t G_t G_r} h_p$ , then, the channel fading coefficient is defined as  $h = \nu h_f$ , where  $h_f$  is the complex small-scale fading and  $h_p$  represents the THz-band free-space path loss, consisting

of both spreading and molecular absorption losses, expressed as [4]

$$h_p = \left( \frac{c}{4\pi f d} \right)^{\frac{\varrho}{2}} \exp \left( -\frac{K_{\text{abs}} d}{2} \right),$$

where  $c$  is the speed of light,  $f$  is the operating frequency,  $d$  is the communication distance, and  $K_{\text{abs}}$  is the molecular absorption coefficient (more details in [4]). In measurement-based sub-THz/THz works [4], [5], the path loss exponent,  $\varrho$ , is best-fit to 2.  $P_t$  denotes the transmit power, and  $G_t$  and  $G_r$  represent the gains of the transmit and receive antennas, respectively. For indoor THz channels, we use the  $\alpha$ - $\mu$ -distribution to represent the magnitude of  $h_f$ , where its probability density function (PDF) is expressed as [14]

$$f_{|h_f|}(y) = \frac{\alpha \mu^\mu y^{\alpha \mu - 1}}{\hat{Z}^{\alpha \mu} \Gamma(\mu)} \exp(-\mu y^\alpha / \hat{Z}^\alpha), \quad (2)$$

where  $\alpha > 0$  is a fading parameter,  $\mu$  is the normalized variance of the fading channel, and  $\hat{Z} = \sqrt{\mathbb{E}(|h_f|^\alpha)}$  is the  $\alpha$  root mean value of the fading channel. Using (2), the PDF of  $h$  can thus be expressed as

$$f_{|h|}(y) = \frac{1}{|y|} f_{|h_f|} \left( \frac{|y|}{\sqrt{y}} \right) = \frac{\alpha \mu^\mu y^{\alpha \mu - 1}}{(\hat{Z} \sqrt{y})^{\alpha \mu} \Gamma(\mu)} \exp(-\mu y^\alpha / (\sqrt{y} \hat{Z})^\alpha). \quad (3)$$

To determine the distribution of  $|h|^2$ , we use the property  $f_Y(y) = f_X(g^{-1}(y)) \left| \frac{d}{dy} g^{-1}(y) \right|$ , for  $Y = X^2 = g(X)$ , which results in,

$$f_{|h|^2}(y) = \frac{\alpha \mu^\mu}{2(\hat{Z} \sqrt{y})^{\alpha \mu} \Gamma(\mu)} y^{\frac{\alpha \mu}{2} - 1} \exp\left(-\mu y^{\alpha/2} / (\sqrt{y} \hat{Z})^\alpha\right). \quad (4)$$

A more parameterized form of the  $\alpha$ - $\mu$  distribution is presented in [10],

$$f_{|h_f|}(x) = \frac{\alpha \beta^{\alpha \mu}}{\bar{x}^{\alpha \mu} \Gamma(\mu)} x^{\alpha \mu - 1} \exp\left(-\left(\beta \frac{x}{\bar{x}}\right)^\alpha\right), \quad (5)$$

where  $\bar{x} = E\{h_f\}$  is the average of  $h_f$  and  $\beta = \frac{\Gamma(\mu + \frac{1}{\alpha})}{\Gamma(\mu)}$ . By applying a similar derivation to that used for (2), the PDF of  $|h|^2$  based on (5) is obtained as

$$f_{|h|^2}(y) = \frac{\alpha \beta^{\alpha \mu}}{2(\bar{x} \sqrt{y})^{\alpha \mu} \Gamma(\mu)} y^{\frac{\alpha \mu}{2} - 1} \exp\left(-\left(\beta \frac{\sqrt{y}}{\bar{x} \sqrt{y}}\right)^\alpha\right). \quad (6)$$

The two PDF forms of the  $\alpha$ - $\mu$  distribution enable different analytical approaches and use cases, as detailed in the following sections.

### III. PROBLEM FORMULATION

We consider  $L \geq 1$  uses of the THz channel and assume an MRC receiver with perfect channel state information (CSI). The simplest code employed is a repetition code, where  $x_l = x_1$  for  $l = 1, \dots, L$ . The received signal is expressed as [7]

$$\tilde{r} = \frac{\mathbf{h}^*}{\|\mathbf{h}\|} \mathbf{r} = \frac{\mathbf{h}^*}{\|\mathbf{h}\|} (\mathbf{h} x + \mathbf{n}) = \|\mathbf{h}\| x + w, \quad (7)$$

where  $\mathbf{r} = [r_1, \dots, r_L]^T$ ,  $\mathbf{h} = [h_1, \dots, h_L]^T$ , and  $\mathbf{n} = [n_1, \dots, n_L]^T$ , and where  $w = \frac{\mathbf{h}^*}{\|\mathbf{h}\|} \mathbf{n} \sim \mathcal{CN}(0, N_0)$ . We define the instantaneous SNR at the receiver, relative to the channel power, as

$$\gamma = \frac{E_s \|\mathbf{h}\|^2}{N_0} = \Upsilon \|\mathbf{h}\|^2, \quad \|\mathbf{h}\|^2 = \sum_{j=1}^L |h_j|^2, \quad (8)$$

where  $\Upsilon = \frac{E_s}{N_0}$ ,  $E_s$  is the energy per symbol, and each  $|h_j|^2$  is distributed either according to (4) or to (6).

To analyze the diversity gain, we derive expressions for the bit error probability in the form  $\text{Pr}_e = \kappa_1 \Upsilon^{-\kappa_2} + o(\Upsilon^{-\kappa_2})$  in the high SNR regime (high  $\Upsilon$ ), where  $\kappa_1, \kappa_2 > 0$ . To this end, we consider two approaches.

- 1- The first approach, proposed in [7], consists of approximating  $\text{Pr}_e$  at high  $\Upsilon$  as

$$\text{Pr}_e \approx \text{Pr}\left(\|\mathbf{h}\|^2 \leq \frac{1}{\Upsilon}\right). \quad (9)$$

At high  $\Upsilon$ , the PDF of  $\|\mathbf{h}\|^2$  can be approximated for small values, enabling the derivation of closed-form expressions for  $\text{Pr}_e$ . We note that this method gives the value of  $\kappa_2$ , but fails to determine the exact value of  $\kappa_1$ .

- 2- The second approach is to compute the exact  $\text{Pr}_e$  [8]:

$$\text{Pr}_e = \mathbb{E}_{\|\mathbf{h}\|^2} \left[ Q\left(\sqrt{\Upsilon \|\mathbf{h}\|^2}\right) \right] = \int_0^\infty Q(\sqrt{\Upsilon x}) f_{\|\mathbf{h}\|^2}(x) dx. \quad (10)$$

This method fully characterizes  $\text{Pr}_e$  as a function of SNR  $\Upsilon$ . In the first order approximation, both  $\kappa_1$  and  $\kappa_2$  are determined.

We note that both methods require knowledge of the PDF of  $\|\mathbf{h}\|^2$  as implied by (9) and (10).

### IV. DIVERSITY ANALYSIS

In this section, we derive the error probability,  $\text{Pr}_e$ , using both methods as outlined in Section III. The analysis is carried out for the THz indoor channel model using (4) and (6).

#### A. The First $\alpha$ - $\mu$ Model

We first analyze the THz  $\alpha$ - $\mu$  indoor channel model following the definition in (3). To find the PDF of  $\|\mathbf{h}\|^2$ , we rewrite the PDF in (4) as

$$f_{|h|^2}(y) = \frac{\bar{\alpha} \mu^\mu y^{\bar{\alpha} \mu - 1}}{\bar{Z}^{\bar{\alpha} \mu} \Gamma(\mu)} \exp\left(-\mu \left(\frac{y}{\bar{Z}}\right)^{\bar{\alpha}}\right), \quad (11)$$

where  $\bar{\alpha} = \frac{\alpha}{2}$  and  $\bar{Z} = (\hat{Z} \sqrt{y})^2$ . It can be seen that the PDF in (11) follows an  $\alpha$ - $\mu$  distribution but with modified parameters. The exact PDF of the sum of independent and identically distributed (i.i.d.)  $\alpha$ - $\mu$  distributed random variables is derived in [9]:

$$f_{\|\mathbf{h}\|^2}(y) = \left( \frac{\bar{\alpha} \mu^\mu}{\Gamma(\mu) \bar{Z}^{\bar{\alpha} \mu}} \right)^L \sum_{i=0}^{\infty} \frac{\delta_i y^{i \bar{\alpha} + \bar{\alpha} \mu L - 1}}{i \Gamma(i \bar{\alpha} + L \mu \bar{\alpha})}, \quad (12)$$

where the coefficients  $\delta_i$  are determined as

$$\delta_i = \begin{cases} \left( \Gamma(\bar{\alpha} \mu) \right)^L, & i = 0 \\ \sum_{\ell=1}^i \frac{\delta_{i-\ell} (\ell L + \ell - i) \Gamma(\bar{\alpha}(\ell + \mu)) \left( -\mu \left( \frac{1}{\bar{Z}} \right)^{\bar{\alpha}} \right)^\ell}{i \Gamma(\bar{\alpha} \mu) \ell!}, & i \geq 1. \end{cases} \quad (13)$$

Given the PDF of  $\|\mathbf{h}\|^2$ , we proceed to find  $\text{Pr}_e$ .

1) *Approximation Method:* As proposed in [7], finding the exponent  $\kappa_2$  requires approximating the PDF,  $f_{\|\mathbf{h}\|^2}(y)$ , for small values of  $y$ . For such small  $y$  values in (12), the term with the smallest exponent of  $y$  dominates the series. This

corresponds to the  $i = 0$  term in the summation. Thus, the first order approximation becomes:

$$f_{\|\mathbf{h}\|^2}(y) = \left( \frac{\bar{\alpha}\mu^\mu \Gamma(\bar{\alpha}\mu)}{\Gamma(\mu)\bar{Z}^{\bar{\alpha}\mu}} \right)^L \frac{y^{\bar{\alpha}\mu L-1}}{\Gamma(L\mu\bar{\alpha})} + o\left(y^{\bar{\alpha}\mu L-1}\right). \quad (14)$$

Evaluating (9) for large  $\Upsilon$  results in

$$\begin{aligned} \Pr\left(\|\mathbf{h}\|^2 \leq \frac{1}{\Upsilon}\right) &= \int_0^{\frac{1}{\Upsilon}} f_{\|\mathbf{h}\|^2}(y) dy \\ &= \left( \frac{\bar{\alpha}\mu^\mu \Gamma(\bar{\alpha}\mu)}{\Gamma(\mu)\bar{Z}^{\bar{\alpha}\mu}} \right)^L \frac{\Upsilon^{-\bar{\alpha}\mu L}}{\Gamma(\bar{\alpha}\mu L+1)} + o\left(\Upsilon^{-\bar{\alpha}\mu L}\right), \end{aligned} \quad (15)$$

where the interchange in the order of the integral and the small-o notation can be justified by the Lebesgue's dominated convergence theorem (DCT). The diversity exponent is given by  $\kappa_2 = \bar{\alpha}\mu L = \frac{\alpha\mu}{2}L$ , highlighting its dependence on the parameters  $\alpha$ ,  $\mu$ , and  $L$ .

2) *Exact Method:* Replacing (12) in (10),

$$\begin{aligned} \Pr_e &= \left( \frac{\bar{\alpha}\mu^\mu}{\Gamma(\mu)\bar{Z}^{\bar{\alpha}\mu}} \right)^L \sum_{i=0}^{\infty} \frac{\delta_i}{\Gamma(\varphi_i)} \int_0^{\infty} x^{\varphi_i-1} Q(\sqrt{\Upsilon}x) dx, \\ &\stackrel{(a)}{=} \left( \frac{\bar{\alpha}\mu^\mu}{\Gamma(\mu)\bar{Z}^{\bar{\alpha}\mu}} \right)^L \sum_{i=0}^{\infty} \frac{\delta_i}{2\Gamma(\varphi_i)} \int_0^{\infty} x^{\varphi_i-1} \operatorname{erfc}\left(\frac{\sqrt{\Upsilon}x}{\sqrt{2}}\right) dx, \\ &\stackrel{(b)}{=} \left( \frac{\bar{\alpha}\mu^\mu}{\Gamma(\mu)\bar{Z}^{\bar{\alpha}\mu}} \right)^L \sum_{i=0}^{\infty} \frac{\delta_i}{\Gamma(\varphi_i)} \int_0^{\infty} t^{2\varphi_i-1} \operatorname{erfc}\left(\frac{\sqrt{\Upsilon}}{\sqrt{2}}t\right) dt, \\ &\stackrel{(c)}{=} \left( \frac{\bar{\alpha}\mu^\mu}{\Gamma(\mu)\bar{Z}^{\bar{\alpha}\mu}} \right)^L \sum_{i=0}^{\infty} \frac{\delta_i 2^{-\varphi_i} \Gamma(\varphi_i + \frac{1}{2})}{\Gamma(\varphi_i + 1) \sqrt{\pi}} \Upsilon^{-\varphi_i}, \end{aligned} \quad (16)$$

where  $\varphi_i \triangleq i\bar{\alpha} + \bar{\alpha}\mu L$ . In step (a), the Q-function is expressed in terms of the complementary error function  $\operatorname{erfc}(\cdot)$  using the identity  $Q(a\sqrt{x}) = \frac{1}{2}\operatorname{erfc}\left(\frac{\sqrt{a^2x}}{2}\right)$ . Step (b) is due to the change of variable  $t = \sqrt{x}$ . The integral term in step (b) is replaced by its closed-form expression found in [15, Eq. 2.8.2.1]; this justifies step (c). Equation (16) quantifies the exact behavior of  $\Pr_e$  as a function of  $\Upsilon$ . For  $\Upsilon \rightarrow \infty$ ,  $\Pr_e$  is governed in the first order by  $\Upsilon^{-\varphi_0}$ , where  $\varphi_0 = \bar{\alpha}\mu L$ . Therefore,

$$\Pr_{e\Upsilon \rightarrow \infty} = \left( \frac{\bar{\alpha}\mu^\mu \Gamma(\bar{\alpha}\mu)}{\Gamma(\mu)\bar{Z}^{\bar{\alpha}\mu}} \right)^L \frac{2^{-\varphi_0} \Gamma(\varphi_0 + \frac{1}{2})}{\Gamma(\varphi_0 + 1) \sqrt{\pi}} \Upsilon^{-\varphi_0} + o\left(\Upsilon^{-\varphi_0}\right). \quad (17)$$

Equation (17) implies that  $\kappa_2 = \varphi_0 = \bar{\alpha}\mu L = \frac{\alpha\mu}{2}L$ , a result which is similar to that obtained using the approximation method. Moreover, the multiplicative constant  $\kappa_1 = \left( \frac{\bar{\alpha}\mu^\mu \Gamma(\bar{\alpha}\mu)}{\Gamma(\mu)\bar{Z}^{\bar{\alpha}\mu}} \right)^L \frac{2^{-\varphi_0} \Gamma(\varphi_0 + \frac{1}{2})}{\Gamma(\varphi_0 + 1) \sqrt{\pi}}$  is perfectly determined here.

### B. The Second $\alpha$ - $\mu$ Model

We examine the THz  $\alpha$ - $\mu$  indoor channel model of (6). To derive the PDF of  $\|\mathbf{h}\|^2$  in this case, we use the result of [16] where it has been shown that

$$f_{\|\mathbf{h}\|^2}(y) \approx \sum_{m=1}^{\Psi} \frac{c_m \bar{\alpha} \bar{\beta}^{\bar{\alpha}\bar{\mu}} y^{\bar{\alpha}\bar{\mu}-1}}{(\omega_m \bar{z})^{\bar{\alpha}\bar{\mu}} \Gamma(\bar{\mu})} e^{-\left(\bar{\beta} \frac{y}{\omega_m \bar{z}}\right)^{\bar{\alpha}}}, \quad (18)$$

where

$$\bar{\alpha} = \frac{\alpha}{2}, \quad \bar{\mu} = \sum_{i=1}^L \mu_i, \quad \bar{\beta} = \frac{\Gamma\left(\bar{\mu} + \frac{1}{\bar{\alpha}}\right)}{\Gamma(\bar{\mu})}, \quad \bar{z} = \sum_{i=1}^L (\bar{x}_i \nu)^2.$$

For any arbitrary integer,  $\Psi$ , the parameters  $c_m$  and  $\omega_m$  are determined by solving the system of linear equations:

$$\begin{aligned} \sum_{m=1}^{\Psi} c_m \omega_m^n &= \frac{\mathbb{E}[Z^n]}{\mathbb{E}^n[Z]} \xi^{(n)}, \quad n = 0, 1, 2, \dots, 2M-2, \\ \sum_{m=1}^{\Psi} \frac{c_m}{\omega_m^{\bar{\alpha}\bar{\mu}}} &= \bar{\alpha}^{L-1} \frac{\bar{z}^{\bar{\alpha}\bar{\mu}} \Gamma(\bar{\mu})}{\bar{\beta}^{\bar{\alpha}\bar{\mu}} \Gamma(\bar{\alpha}\bar{\mu})} \times \prod_{i=1}^L \frac{\beta_i^{\bar{\alpha}\mu_i} \Gamma(\bar{\alpha}\mu_i)}{\bar{y}_i^{\bar{\alpha}\mu_i} \Gamma(\mu_i)}. \end{aligned}$$

Here,  $\xi^{(n)}$  is defined as:

$$\xi^{(n)} = \frac{\Gamma(\bar{\mu} + \frac{n}{\bar{\alpha}}) \Gamma^{n-1}(\bar{\mu})}{\Gamma^n(\bar{\mu} + \frac{1}{\bar{\alpha}})}.$$

To derive  $\mathbb{E}[Z^n]$ , we use the following formula, which relies on the individual terms of the summation in the random variable  $Z$ :

$$\begin{aligned} E(Z^n) &= \sum_{n_1=0}^n \sum_{n_2=0}^{n_1} \dots \sum_{n_{L-1}=0}^{n_{L-2}} \binom{n}{n_1} \binom{n_1}{n_2} \dots \binom{n_{L-2}}{n_{L-1}} \\ &\quad \times E(Y_1^{n-n_1}) E(Y_2^{n_1-n_2}) \dots E(Y_L^{n_{L-1}}). \end{aligned} \quad (19)$$

We proceed next to finding  $\kappa_1$  and  $\kappa_2$  for the THz model in (6), using (18).

1) *Approximation Method:* When  $y$  is sufficiently small in (18), we use the following approximation,

$$\exp(y) \approx 1 + o(y),$$

and (18) boils down to

$$f_{\|\mathbf{h}\|^2}(y) \approx \sum_{m=1}^{\Psi} \Lambda_m y^{\bar{\alpha}\bar{\mu}-1} + o\left(y^{\bar{\alpha}\bar{\mu}-1}\right), \quad (20)$$

where

$$\Lambda_m = \frac{c_m \bar{\alpha} \bar{\beta}^{\bar{\alpha}\bar{\mu}}}{(\omega_m \bar{z})^{\bar{\alpha}\bar{\mu}} \Gamma(\bar{\mu})}.$$

This implies that, for large values of  $\Upsilon$ ,

$$\begin{aligned} \Pr\left(\|\mathbf{h}\|^2 \leq \frac{1}{\Upsilon}\right) &= \sum_{m=1}^{\Psi} \Lambda_m \int_0^{\frac{1}{\Upsilon}} y^{\bar{\alpha}\bar{\mu}-1} dy + \int_0^{\frac{1}{\Upsilon}} o\left(y^{\bar{\alpha}\bar{\mu}-1}\right) dy \\ &\approx \sum_{m=1}^{\Psi} \Lambda_m \frac{\Upsilon^{-\bar{\alpha}\bar{\mu}}}{\bar{\alpha}\bar{\mu}} + o\left(\Upsilon^{-\bar{\alpha}\bar{\mu}}\right), \end{aligned} \quad (21)$$

Equation (21) implies that the diversity exponent is equal to  $\kappa_2 = \bar{\alpha}\bar{\mu} = \frac{\alpha}{2} \sum_{j=1}^L \mu_j$ . This quantifies the rate at which the probability of error decreases with increasing SNR, where higher values of  $\bar{\alpha}\bar{\mu}$  imply higher diversity gains.

2) *Exact Method:* Starting with (10) and using (18), we obtain

$$\Pr_e = \sum_{m=1}^{\Psi} \frac{\Lambda_m}{2} \int_0^{\infty} y^{\bar{\alpha}\bar{\mu}-1} \operatorname{erfc}\left(\frac{\sqrt{\Upsilon}y}{\sqrt{2}}\right) \exp\left(-\bar{\beta} \frac{y}{\omega_m \bar{z}}\right)^{\bar{\alpha}} dy, \quad (22)$$

where, to compute this integral, we follow the procedure outlined in [16, Eq. 30]. A step-by-step solution is provided therein for further details. As a result, we obtain:

$$\begin{aligned} \Pr_e &= \sum_{m=1}^{\Psi} \frac{\Lambda_m}{2\sqrt{\pi}} \left( \frac{\Upsilon}{2} \right)^{-\bar{\alpha}\bar{\mu}} \\ &\quad \times H_{2,2}^{1,2} \left[ \left( \frac{2\bar{\beta}}{\Upsilon \omega_m \bar{z}} \right)^{\bar{\alpha}} \middle| \begin{array}{c} (1 - \bar{\alpha}\bar{\mu}, \bar{\alpha})(\frac{1}{2} - \bar{\alpha}\bar{\mu}, \bar{\alpha}) \\ (0, 1) (-\bar{\alpha}\bar{\mu}, \bar{\alpha}\bar{\mu}) \end{array} \right]. \end{aligned} \quad (23)$$

For  $\Upsilon \rightarrow \infty$ , the term  $t = \left(\frac{2\bar{\beta}}{\Upsilon \omega_m \bar{z}}\right)^{\bar{\alpha}}$  in (23) approaches

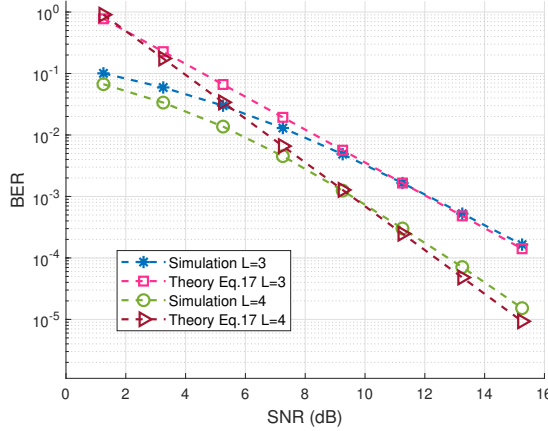


Fig. 1. BER versus SNR for  $\alpha = 3.45388$ ,  $\mu = 0.51571$ , and  $L = 3, 4$

zero. In [13, Appendix F], the authors conducted an asymptotic analysis of the Fox H-function  $H_{p,q}^{m,n}(t|)$  in the regime where  $t \rightarrow 0$  to obtain

$$H_{p,q}^{m,n}(z) = \sum_{j=1}^m \left[ h_j^* z^{b_j/\beta_j} + O\left(z^{(b_j+1)/\beta_j}\right) \right] \quad (z \rightarrow 0), \quad (24)$$

$$h_j^* = \frac{\prod_{i=1, i \neq j}^p \Gamma\left(b_i - \frac{b_j \beta_i}{\beta_j}\right) \prod_{i=1}^n \Gamma\left(1 - a_i + \frac{b_j \alpha_i}{\beta_j}\right)}{\beta_j \prod_{i=n+1}^p \Gamma\left(a_i - \frac{b_j \alpha_i}{\beta_j}\right) \prod_{i=m+1}^q \Gamma\left(1 - b_i + \frac{b_j \beta_i}{\beta_j}\right)}.$$

Using the asymptotic expression (24), for  $\Upsilon \rightarrow \infty$ , equation (23) becomes

$$\Pr_{\epsilon \Upsilon \rightarrow \infty} \approx \frac{2^{\bar{\alpha}\bar{\mu}-1}}{\sqrt{\pi}} \left( \sum_{m=1}^{\Psi} \Lambda_m \right) \Upsilon^{-\bar{\alpha}\bar{\mu}} \left[ h_1^* + O\left(\frac{2\bar{\beta}}{\Upsilon \omega_m \bar{z}}\right) \right]. \quad (25)$$

As observed, the diversity exponent is given by  $\kappa_2 = \bar{\alpha}\bar{\mu} = \frac{\alpha}{2} \sum_{j=1}^L \mu_j$ . This result is consistent with the outcome obtained using the approximation method in (21), thereby validating the robustness of our proposed framework. In addition, we find that  $\kappa_1 = \frac{2^{\bar{\alpha}\bar{\mu}-1}}{\sqrt{\pi}} \left( \sum_{m=1}^{\Psi} \Lambda_m \right) h_1^*$ .

## V. SIMULATION RESULTS

We validate the theoretical analysis through numerical simulations, using a MATLAB-based simulator configured with parameters derived from validated THz channel measurements in the literature [5]. The simulator accurately captures key channel characteristics and models small-scale fading using the  $\alpha$ - $\mu$  distribution. We define  $N_0 = k_B T B$ , where  $k_B$  the Boltzmann constant,  $B$  is the system bandwidth, and  $T = 300$  K is the system temperature. Simulations are performed under BPSK modulation with  $f = 0.142$  THz,  $B = 4$  GHz. The used antenna gains are  $G_r = 19$  dBi and  $G_t = 0$  dBi [17]. We adjust  $P_t$  to vary the SNR range. For small-scale fading, we evaluate the  $\alpha$ - $\mu$  model from [5] with different parameters.

Figure 1 depicts the BER performance for the  $\alpha$ - $\mu$  distribution with parameters  $\alpha = 3.45388$  and  $\mu = 0.51571$ , as derived from experimental measurements in [5]. The results are shown for two diversity configurations:  $L = 3$  and  $L = 4$ . The theoretical analysis is based on the exact

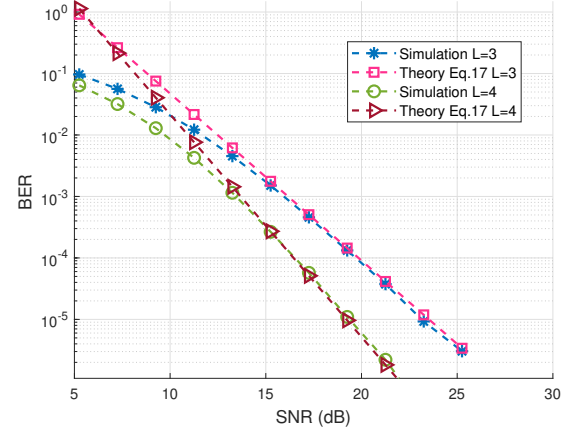


Fig. 2. BER versus SNR for  $\alpha = 2.92801$ ,  $\mu = 0.61844$ , and  $L = 3, 4$ .

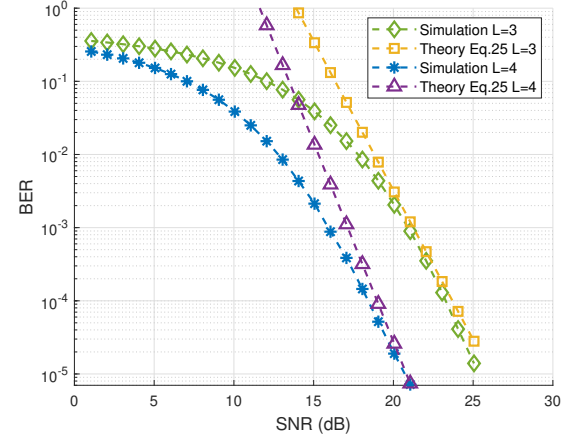


Fig. 3. BER versus SNR for  $L = 3, 4$ . Theory is in reference to (25).

method as outlined in (17). The approximation method in (15) predicts the same diversity exponent  $\kappa_2$ , and its accuracy is thus captured by the plot of the exact method. The close agreement between (17) and simulation results in the high SNR regime confirms the accuracy of our theoretical analysis. As anticipated, increasing the number of diversity branches  $L$  leads to significant performance improvements, highlighting the effectiveness of diversity in mitigating fading effects. In addition, we plot in figure 2 an evaluation for another set of parameters,  $\alpha = 2.92801$  and  $\mu = 0.61844$  [5].

Furthermore, Figure 3 presents simulation results for the  $\alpha$ - $\mu$  distribution described in (6), using the parameters from [5]. As observed, the theoretical and simulated curves show a close match in the high SNR regime. The theoretical results, obtained from the exact analytical expression in (25), confirm the accuracy of the simulations. Similar to the previous case, the approximation method result in (21) predicts the same diversity gain  $\kappa_2 = \frac{\alpha}{2} \sum_{i=1}^L \mu_i$ . The results again demonstrate a strong consistency between the theoretical results and the simulation outcomes at high SNR, thus further confirming the

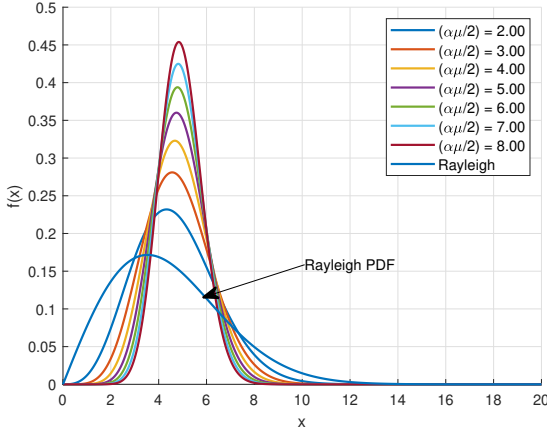


Fig. 4. PDF of  $\alpha$ - $\mu$  distribution for fixed  $\alpha = 2$  and varying  $\mu$ .

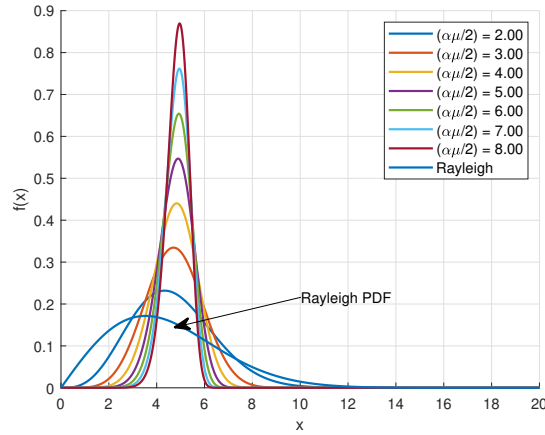


Fig. 5. PDF of  $\alpha$ - $\mu$  distribution for fixed  $\mu = 2$  and varying  $\alpha$ .

robustness and reliability of our proposed framework.

The decrease of the error probability,  $\text{Pr}_e$ , with  $\kappa_2 = \frac{\alpha\mu}{2}L$  as a function of SNR is attributed to the fact that the  $\alpha$ - $\mu$  PDF becomes more concentrated as the product  $\alpha\mu$  increases. In figures 4 and 5, we plot the  $\alpha$ - $\mu$  PDF for various values of  $\mu$  and  $\alpha$  respectively. The figures capture the effect of the product  $\alpha\mu$  on the density function: the greater the product of  $\alpha\mu$ , the higher the concentration of the PDF and thus the better the channel. This in turn implies that as the product  $\alpha\mu$  increases, the diversity exponent should be higher, since a higher concentration of the fading PDF leads to having more reliable signal recovery. Our analysis shows that the diversity exponent  $\kappa_2$  is indeed proportional to the product  $\alpha\mu$ .

## VI. CONCLUSION

In this paper, we present a framework for analyzing diversity in THz communication systems. Unlike existing studies [9], [10] that often assume simplified fading models (limited to

small-scale fading), our approach incorporates the small-scale  $\alpha$ - $\mu$  distribution along with free-space path loss, enabling a more accurate representation of the THz system model. We develop two complementary methods for error probability computation and demonstrate their robustness through both analytical and numerical results. Our analysis reveals that the concentration properties of the  $\alpha$ - $\mu$  distribution play a critical role in diversity gain: sharper clustering of multipath components significantly improves signal recovery reliability, particularly in dense scattering environments. Furthermore, we show that optimal diversity performance depends not only on the number of antennas but also on the fading parameters. These insights provide practical guidelines for designing high-performance THz systems under realistic channel conditions.

## REFERENCES

- [1] H. Sarieddeen, M.-S. Alouini, and T. Y. Al-Naffouri, "An overview of signal processing techniques for terahertz communications," *Proc. IEEE*, vol. 109, no. 10, pp. 1628–1665, 2021.
- [2] J. M. Jornet *et al.*, "The evolution of applications, hardware design, and channel modeling for terahertz (THz) band communications and sensing: Ready for 6G?" *Proc. IEEE*, pp. 1–32, 2024.
- [3] F. Sheikhi *et al.*, "THz measurements, antennas, and simulations: From the past to the future," *IEEE Journal of Microwaves*, vol. 3, no. 1, pp. 289–304, 2022.
- [4] S. Tarboush, H. Sarieddeen, H. Chen, M. H. Loukil, H. Jemaa, M.-S. Alouini, and T. Y. Al-Naffouri, "TeraMIMO: A channel simulator for wideband ultra-massive MIMO terahertz communications," *IEEE Transactions on Vehicular Technology*, vol. 70, no. 12, pp. 12 325–12 341, 2021.
- [5] E. N. Papasotiriou *et al.*, "An experimentally validated fading model for THz wireless systems," *Sci. Rep.*, vol. 11, no. 1, p. 18717, 2021.
- [6] A.-A. A. Boulogiorgos, E. N. Papasotiriou, and A. Alexiou, "Analytical performance assessment of THz wireless systems," *IEEE Access*, vol. 7, pp. 11 436–11 453, 2019.
- [7] D. Tse and P. Viswanath, *Fundamentals of wireless communication*. Cambridge university press, 2005.
- [8] M. K. Simon and M.-S. Alouini, *Digital communication over fading channels*. John Wiley & Sons, 2005, vol. 95.
- [9] F. D. Almeida García, F. R. A. Parente, M. D. Yacoub, and J. C. S. S. Filho, "On the exact sum PDF and CDF of  $\alpha$ - $\mu$  variates," *IEEE Transactions on Wireless Communications*, vol. 22, no. 8, pp. 5084–5095, 2023.
- [10] M. Payami and A. Falahati, "Accurate variable-order approximations to the sum of  $\alpha$  –  $\mu$  variates with application to MIMO systems," *IEEE Transactions on Wireless Communications*, vol. 20, no. 3, pp. 1612–1623, 2021.
- [11] A. P. Prudnikov *et al.*, *Integrals and series: Special functions*. CRC press, 1986, vol. 2.
- [12] A. A. Kilbas, *H-transforms: Theory and Applications*. CRC press, 2004.
- [13] H. Jemaa *et al.*, "Performance analysis of outdoor THz links under mixture Gamma fading with misalignment," *IEEE Commun. Lett.*, vol. 28, no. 11, pp. 2668–2672, 2024.
- [14] A. M. Magableh and M. M. Matalgah, "Moment generating function of the generalized  $\alpha$ - $\mu$  distribution with applications," *IEEE Commun. Lett.*, vol. 13, no. 6, pp. 411–413, 2009.
- [15] I. S. Gradshteyn and I. M. Ryzhik, *Table of integrals, series, and products*. Academic press, 2014.
- [16] H. Jemaa *et al.*, "Performance and complexity analysis of terahertz-band mimo detection," 2025. [Online]. Available: <https://arxiv.org/abs/2504.05268>
- [17] E. N. Papasotiriou *et al.*, "Outdoor THz fading modeling by means of Gaussian and Gamma mixture distributions," *Sci. Rep.*, vol. 13, no. 1, p. 6385, 2023.